

Supplementary Information for “Signatures of hot hydrogen in the atmosphere of the extrasolar planet HD209458b” (*Nature* # 2006-09-10792)

Gilda E. Ballester¹ & David K. Sing^{1,2}

¹Lunar and Planetary Laboratory, University of Arizona, Sonett Space Sciences Building, Tucson, Arizona, 85721-0063, USA

²Institut d’Astrophysique de Paris, CNRS/UPMC, 98 bis Boulevard Arago, F-75014 Paris, France

This Supplementary Information provides details about data reduction, derivation of the photometric light curves, corrections to systematic instrumental effects, corrections to the transit spectra accounting for the stellar limb-darkening, and calculation of the Balmer jump absorption from hot ($n = 2$) hydrogen based on a published model of HD209458b’s upper atmosphere. It also contains three related figures.

1 Supplementary methods

Data reduction: The HST STIS G430L observations of HD209458 are detailed in Knutson *et al.* (2006)¹⁰ and consist of 22-second integrations during two planetary transits on May 03 and June 25, 2003. The two observing series spanned five HST orbits each, and were designed, along with G750L observations, to sample a complete transit. The spectra were taken with a wide $52'' \times 2''$ slit in order to produce photometric spectra with minimal slit losses⁹.

The dataset was pipeline-reduced with CALSTIS and cleaned for cosmic ray detections before performing spectral extractions. The aperture extraction was done in IRAF software with a 17-pixel-wide aperture, previously found to minimize RMS variations⁹, which is also close to the average aperture size used by Knutson *et al.* (2006)¹⁰. The extracted spectra were then flux calibrated using the latest G430L sensitivity curve.

Photometric light curves and corrections to systematic instrumental effects: The STIS G430L spectra were used to create photometric time series for two bandpasses. We defined a near-UV/violet bandpass covering 3,000-4,000 Å and a blue bandpass covering 4,400-5,500 Å, both having unity transmission within their respective ranges and zero outside. The flux was inte-

grated within each bandpass per exposure. Both photometric time series show all of the systematic effects expected for this type of HST data⁹, as can be seen in the Supp. Fig. 1. These effects include: (1) a flux decrease over each orbit with an approximate amplitude of 0.1% over 48 minutes; (2) a transit-to-transit difference in scale; and (3) the flux in the first sample of every HST orbit being substantially different (usually smaller) than the average. We corrected these systematic effects in each bandpass and transit separately⁹. First, we fit the out-of-transit time series with a linear function and then divided the entire series by that function, removing the transit-to-transit differences of effect (2). We then fit the out-of-transit orbits, phased with the HST orbital period, with a fourth order polynomial dividing all the orbits by this function as well. This correction removed the in-orbit decrease of effect (1). Finally, we disregarded the first sample in each orbit to correct for effect (3). The resulting photometric time series corrected for systematic instrumental errors can be seen in Fig. 1 of the main text. In addition to correcting the photometric series, the linear and polynomial corrections were also applied directly to each spectrum extracted from each exposure, linearly interpolating between the blue and near-UV/violet corrections over the G430L wavelength region.

Limb-darkening model corrections: In order to produce photometric light curves and a transit flux ratio spectrum directly dependent on the radii of the planet and parent star, we corrected the data for stellar limb-darkening using a method similar to the one reported in Knutson *et al.* (2006)¹⁰. To make the corrections, we used a nonlinear limb-darkening law which has four coefficients, with each being wavelength dependent¹². The coefficients were fit using a Kurucz stellar model and associated spectra for HD209458¹¹ at 17 different angles from center to limb, using the G430L dispersion solution. Each Kurucz model spectrum was first degraded with a Gaussian smoothing of 1.8 pixels FWHM to approximate the G430L resolution. In order to co-align the STIS spectra at zero velocity, each G430L spectrum was first co-aligned in wavelength against the first spectrum obtained and then shifted by 5.187 pixels to match the Kurucz stellar spectra. Thus, every pixel in the G430L spectra could then be corrected for limb-darkening independently. By applying the limb-darkening corrections at the G430L dispersion, stellar absorption features are taken into account, which can have slightly different limb-darkening coefficients than the surrounding continuum. Publicly available computer programs¹² were used along with a stellar radius of $R_{\star} = 1.125 R_{Sun}$ and an inclination angle of $i = 86.929^{\circ}$ to create model photometric transit light curves, fitting for planetary radii at the two photometric bandpasses. By calculating model transit light curves both with and without limb-darkening, we were able to calculate a correction factor and apply it to the dataset, effectively taking out the effects of limb-darkening. In the main

text, the limb-darkening corrected photometric light curves are shown in Fig. 1 (dashed lines), and the corrected transit flux ratio spectrum is shown Fig. 2 (smoothed, center).

Calculation of HI absorption in the Balmer jump: For the calculation, we first used the Boltzmann and Saha equations to calculate the $n = 2$ HI population versus planetary radius (Supp. Fig. 2), using the Yelle (2004, 2006)^{4,5} model values of temperature, HI density, and electron density assuming these values dropped to zero beyond the planet's Roche lobe. We then calculated the tangential column density and associated optical depth versus (projected) radial distance (r) from the planet center, integrating along a $\pm 3.3 R_{pl}$ or smaller column with 100-km steps (Supp. Fig. 3, top). The optical depth was then calculated using the bound-free HI cross section¹⁴. At the wavelengths of interest, the free-free cross section is relatively small, as is the bound-free absorption from the $n = 3$ state, so these were ignored. The optical depth of the Balmer jump versus radial distance, $\tau(r)$, is plotted in Supp. Fig. 3 (bottom). $\tau(r)$ has a sharp peak around $r = 1.09 R_{pl}$. The peak absorbing layer causes appreciable absorption at smaller radial distances due to the line-of-sight through the atmosphere. Above $r = 1.09 R_{pl}$, $\tau(r)$ drops by ~ 4 orders of magnitude in a short distance of $0.06 R_{pl}$.

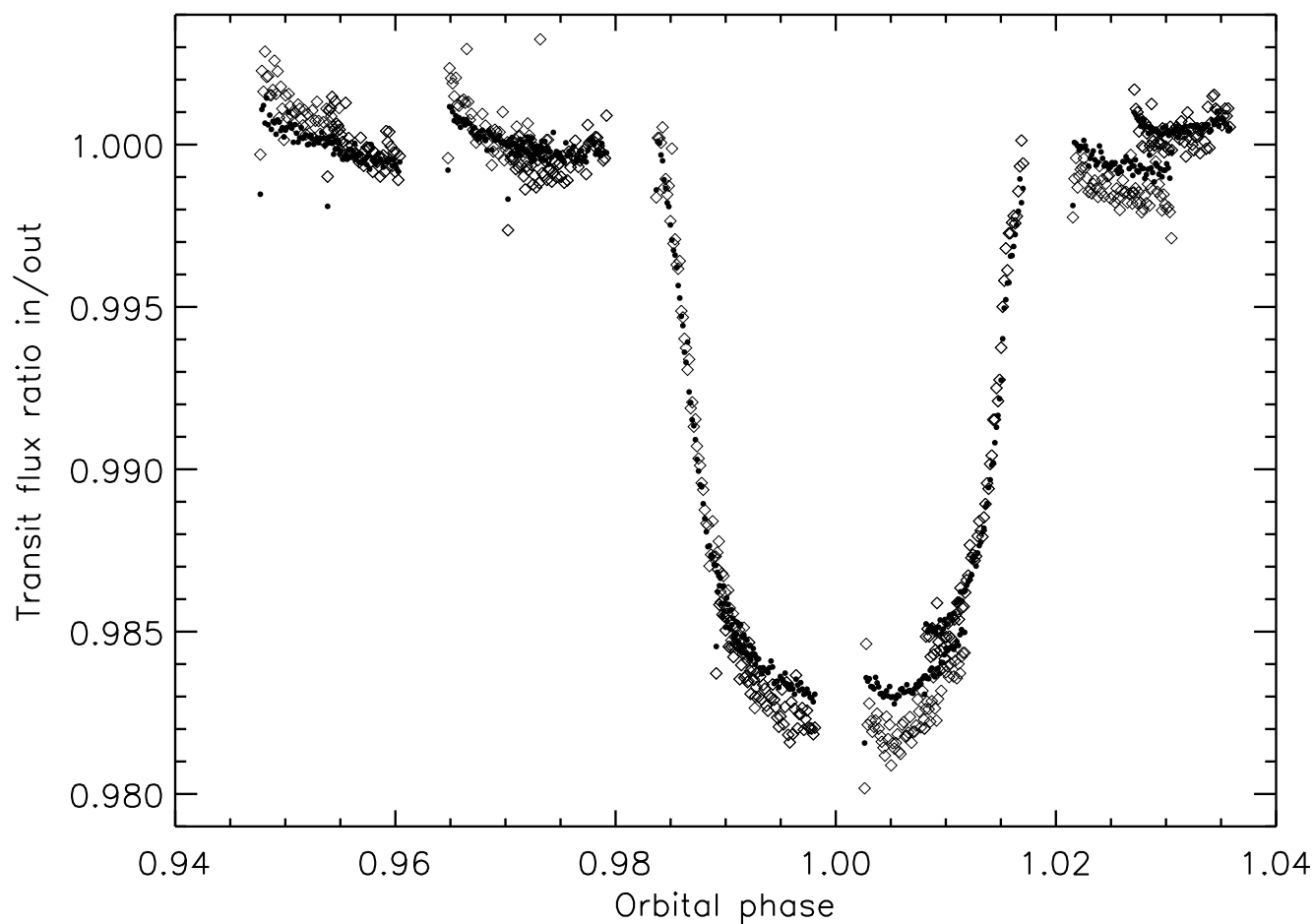
Assuming spherical symmetry, the absorption was then integrated in 100-km-wide annuli out to $r = 3.3 R_{pl}$. Although the area of the annuli increases by a factor of ~ 5 from $r = 1 R_{pl}$ to $r = 3.3 R_{pl}$, this is not a large enough factor to significantly modify the integrated absorption profile as a function of radial distance. Thus, the bulk of the absorption is produced mainly by a significant population of excited hydrogen between $r = 1.08 R_{pl}$ and $r = 1.1 R_{pl}$ (altitude of 8,500 km, $\sim 1,000$ km wide). At this altitude, the absorbing HI layer is in the lower thermosphere of the planet and should be well above the optically opaque layer that defines $1 R_{pl}$ (which possibly, but not necessarily, corresponds to cloud tops).

The net absorption seen while in mid-planetary transit of a uniformly bright stellar disk is expressed as a transit flux ratio, $F_{\lambda,in}/F_{\lambda,out}$. This is calculated, as a function of wavelength, as

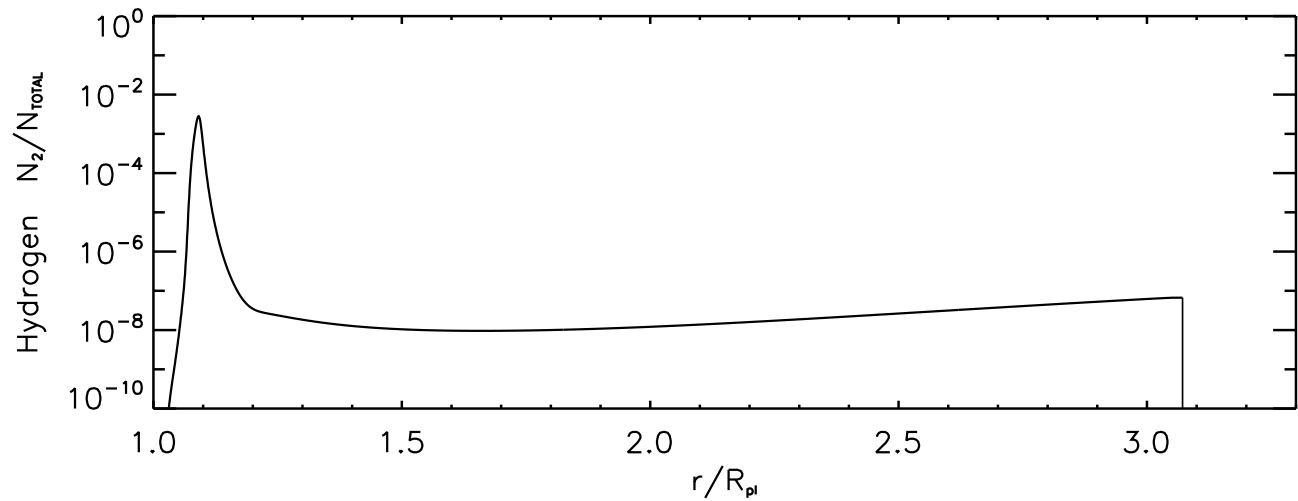
$$\frac{F_{\lambda,in}}{F_{\lambda,out}} = \frac{\int_0^{2\pi} \int_{R_{pl}}^{R'} I_{\lambda} e^{-\tau_{\lambda}(r)} dA + \int_0^{2\pi} \int_{R'}^{R_{\star}} I_{\lambda} dA}{I_{\lambda} \pi R_{\star}^2}, \quad (1)$$

where $dA = r dr d\phi$, $\tau_{\lambda}(r)$ is the optical depth discussed above, and R' is the radial extent of our calculation of the planetary atmospheric absorption ($R' = 3.3 R_{pl}$). The expression assumes that the incoming radiation field, I_{λ} , is normal to the plane of the area of integration, and that it is emitted by a uniform stellar disk. This net calculated absorption can be directly compared to the limb-darkening corrected transit flux ratio derived from the data.

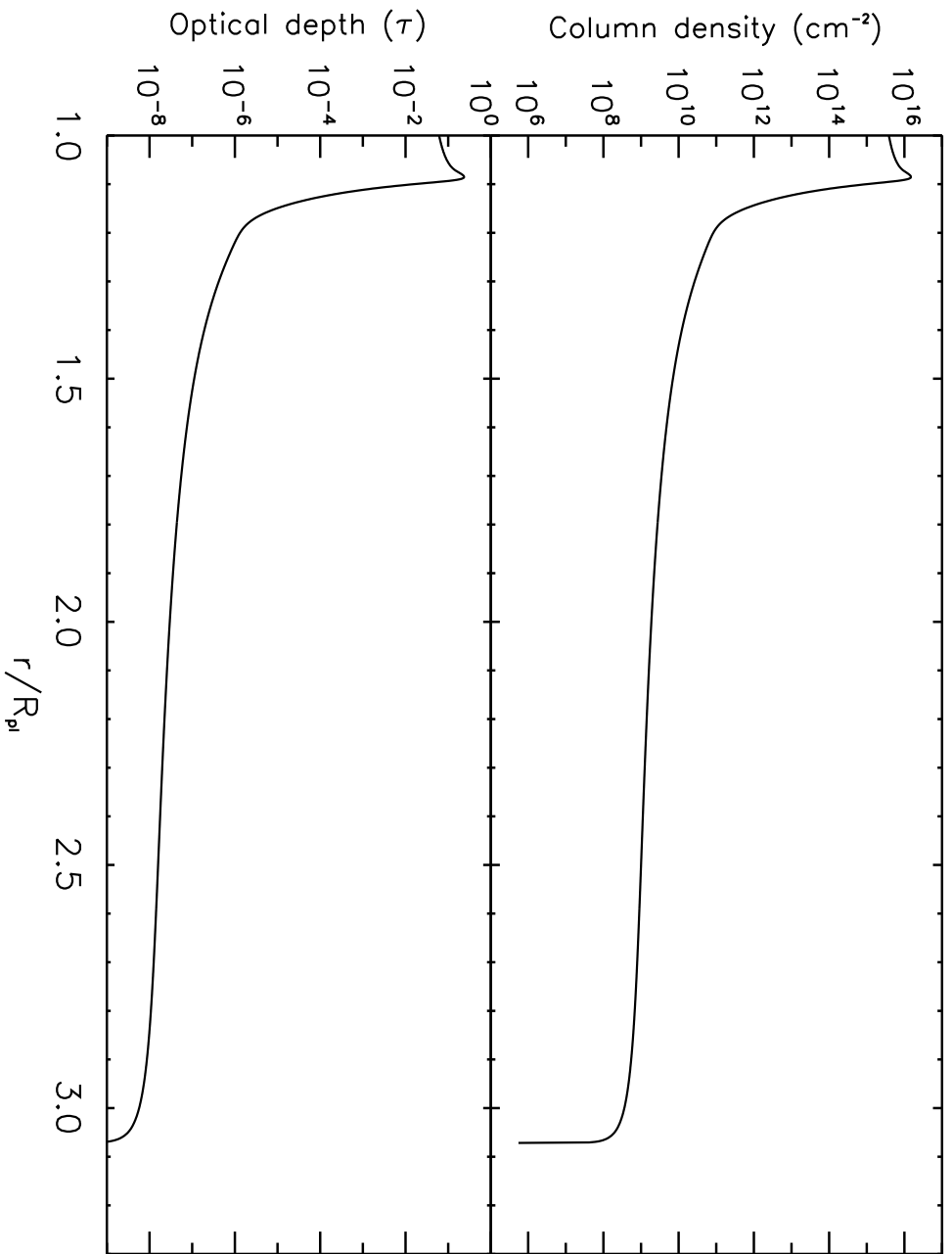
2 Supplementary figures and legends



Supplementary Figure 1 | Photometric transit light curves of HD209458. Shown are the transit STIS G430L light curves at the two photometric bandpasses, near-UV/violet 3,000-4,000 Å (diamonds) and blue 4,500-5,500 Å (filled circles). The data have not been corrected for the systematic instrumental effects described in the Supplementary Methods.



Supplementary Figure 2 | Excited H I number density. Shown is the calculated number density of H I in the first excited state ($n = 2$) relative to the total number of H I atoms plotted as a function of radius, based on the model atmosphere by Yelle^{4,5}.



Supplementary Figure 3 | Excited H I column density and optical depth. Top: Calculated tangential column density of hot ($n = 2$) H I as a function of (projected) planetary radial distance. Bottom: Corresponding atomic hydrogen bound-free optical depth at the Balmer jump at 3,646 Å.